ELSEVIER

Journal of Nuclear Materials 271&272 (1999) 512–517

journal of nuclear materials

Research progress of fusion materials in CIAE

Jinnan Yu *, Changqi Shan

China Institute of Atomic Energy (CIAE), P.O. Box 275-51, Beijing 102413, People's Republic of China

Abstract

The research project of fusion reactor materials in CIAE consists of the first wall materials, plasma-facing component (PFC) materials, tritium technology, HTSC superconductor study and modeling of radiation damage processes. The research activities and some results are given in this paper.

1. Introduction

The fusion energy as an advanced energy source will play a very important role after the middle of the 21st century. The research and development of fusion energy are a key issue in the energy strategy for the next century in China. The R&D program of fusion energy is supported by the National High Technology Project (NHTP). There are two kinds of fusion reactor concepts, inertial and magnetic confinement fusion, and two programs have been supported by NHTP. The short-term Chinese research program of the magnetic confinement fusion concept is aimed at the developing of a fusion–fission hybrid reactor.

Fusion materials studies are an important part of the fusion energy development program in China. The purpose of the study is to found a basis of science and technology for fusion reactor technology and materials development. In order to develop the hybrid reactor based on the domestic ability of manufacturing and knowledge, 316L and 316Ti stainless steel, Cu–25Al alloy, graphite coated by TiC and $LiAlO_2$ are considered to be used as first-wall, divertor, amour and breeder materials, respectively. Considering future development, the performances of SiC_f/SiC, ODS ferritic steel and HTSC superconductors are also investigated. Correspondingly we make the efforts to do modeling work of radiation effects and develop international collaboration.

The research program of fusion materials in CIAE is an important part of fusion materials research and has achieved progress in the following subjects:

1. the synergistic action of high-energy cascades, helium and hydrogen [1–4];
2. developing the cyclic irradiation technique with high energy flux to study irradiation fatigue (irradiation and thermal cycling) [5];
3. Cu-Al25 alloy irradiated by 300-keV Cu^+ ion to simulate the effects of high energy PKA produced by 14-MeV neutrons [6];
4. the performance of $LiAlO_2$ and the tritium permeation barrier of oxides, carbide and nitride and carbide composite coating materials [7–9];
5. radiation effects on the YBCO and Bi-system superconductors [10–12];
6. developing a modified model of microstructural evolution under irradiation and a code for the recoils, fragments, transmutational products spectrum and their distribution in the materials irradiated by neutrons and protons [13–15].

2. Structural materials

The 316L and 316Ti stainless steels (316L and 316Ti SS) are the prime candidate materials for the first wall of hybrid reactor, which is exposed to 14 MeV neutron irradiation, hydrogen and helium ion bombardment. The synergistic action of high-energy cascades and helium induces swelling, blistering and helium embrittlement.

The samples were irradiated by α beam with 1.8 MeV to a fluence of 0.87×10^{18} α/cm^2 at 500°C by the Van de

* Corresponding author. Tel.: +86-10 69357232; fax: +86-10 69357008; e-mail: yujn@sun.ihep.ac.cn

0022-3115/99/$ – see front matter
PII: S0022-3115(98)00725-9

Graaf accelerator and the range, vacancy and particle distribution were calculated by TRIM code. Based on sectioning technology and TEM observation [2,3], the distribution of bubble size and density with depth were measured to investigate the relation between the swelling and damage dose (DPA) for some helium-content/damage-dose ratio, as well as the character of α-particle irradiation. The mean bubble size (nm) along the depth (μm) is shown in Fig. 1. The shapes of mean bubble size–depth curves are similar to those of damage–depth curves. The peak region of mean bubble size approaches the damage peak region (DPR) and its site is at 2.5 μm which is 0.31 μm less than the calculated value of mean range; therefore the content of helium in this region is not too high. Beyond the mean range, the content of helium is the highest, but the bubble size is small. In the DPR, the vacancy concentration is the highest, which makes the cascade influence region more wide to increase the overlapping probability of cascade; the density of bubble nuclei is not too high and the abundant vacancies make the bubble nuclei grow. The result for the synergistic action is that the bubble size is the largest and the bubble density is lower. In contrast to the DPR, beyond the mean range there is abundant helium and the damage rate is lower. The high helium bubble nucleation and the low vacancy concentration suppress bubble nucleus growth. Therefore the bubble size is small. It means that the bubble size mainly depends on the vacancy concentration in the region where the helium occurs, and the action of the helium mainly is to form the nucleus of bubbles(or voids). Beyond a depth of 3 μm, which is the calculated maximum range for the helium, there are no bubbles. This shows that the α-particles are all retained in the implantation region and trapped by the displacement damage to form bubble nuclei.

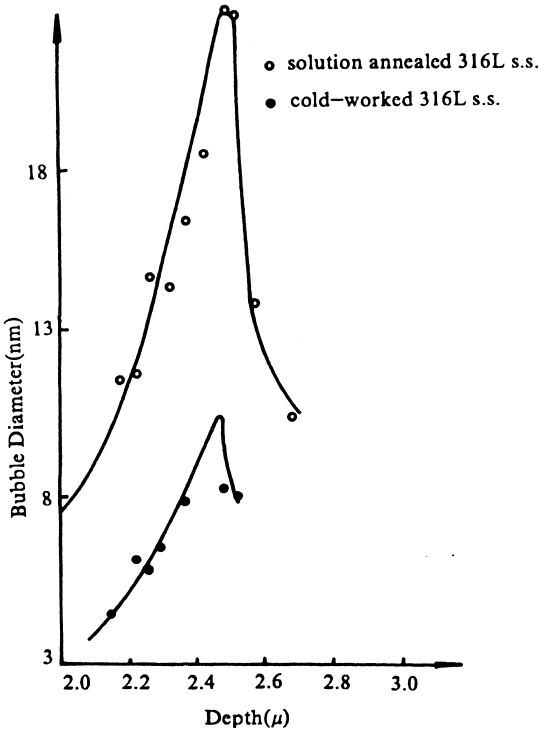

Fig. 1. The mean bubble size (nm) as a function of depth (μm) for the 316L stainless steel irradiated by α beam with 1.8 MeV to a fluence of $0.8\ 7 \times 10^{18}$ α/cm^2 at 500°C.

The experiment for the specimen irradiated with 1.5-MeV proton to a fluence of 3.7024×10^{19} protons/cm^2 at 500°C [1,4] shows that the synergistic action of high-energy cascades and hydrogen induces dense tiny bubble (or void) and the diameter of the bubble is 2–3 nm. The hydrogen substitutes for gaseous impurities (such as soluted oxygen, nitrogen, sulfur and phosphorus) which react with the other components form new phases, such as Cr_2O_3, $(CrFe)_2O_3$, $(Fe_5C_2)28N$, (CrMo)N, $(Fe_2Mo)12H$ and $(FeNi)_9S_8$ [1,4].

The high amount of hydrogen combined with the high energy cascades and helium to induce more damage than that of helium and cascades. The 316L SS specimens irradiated with 27 keV mixed ion beam of helium and hydrogen to the same helium dose (6.4×10^{17}He$^+$/cm^2) at 573 K shows that the mean diameter and density of bubble on the surface, increase with the hydrogen content increase [4]. The data is shown in Table 1. The blister on the specimen #6 only occurs on a few parts of surface, but it is easier to find the blister on the specimen #2 and the blistering is light. The bubbles occur on the surface of specimen #4 everywhere and the blistering is medium. The blistering on the specimen #3 was serious. The blistering increased with hydrogen ions increase.

3. Plasma facing materials

Dispersion strengthened Cu-Al25 alloy has been considered as a candidate high heat flux alloy for fusion applications. A Cu-Al25 alloy containing small Al_2O_3 particles (~4 nm in diameter) was irradiated by 300-keV Cu^+ ion to 10 and 30 dpa with a displacement rate of 3.7×10^{-2} dpa/s at room temperature to simulate the effects of high energy primary knock-on atom (PKA) [6]. Selected area diffraction (SAD) mode was used to study the phase stability of alumina under irradiation. After irradiation to 10 dpa the intensity of reflexes from Al_2O_3 phase decreases considerably in comparison with the state before irradiation; only very weak reflexes from Al_2O_3 phase were observed at the irradiated specimens with 30 dpa. Small Al_2O_3 particles were dissolved under ion irradiation with the fluence. The defect cluster structure formed by irradiation was investigated by

Table 1
The blister at various doses and ratios of helium to hydrogen for the 316L stainless steel irradiated with 27 keV mixed ion beam of helium and hydrogen at 573 K

Specimen	He dose $\times 10^{17}$	Total dose $\times 10^{17}$	Ratio He/H (%)	Mean diameter (mm)	Density $\times 10^{6}$ cm^{-2}
#6	6.4	6.4	no H	0.562	6.97
#2	6.4	21.3	0.30	0.641	20.7
#4	6.4	32	0.20	0.718	18.3
#3	6.4	53.3	0.12	0.680	38.1

dynamical two-beam technology. A large number of small Frank vacancies and interstitial loops (~5 nm in diameter) with different Burgers vector of $a/3\langle 1\ 1\ 1\rangle$ are produced by ion irradiation. At the region adjacent to the irradiation surface the number of vacancy loops is more than that of interstitial ones. This result is in good agreement with the computer simulation result.

An irradiation target chamber with rotatable table and a set of quadrupole magnetic lenses associated with the 14-MeV Short-pulse Electron Linear Accelerator was used to irradiate high heat flux materials. The Electron Gamma Shower Simulation Code (EGS4) was modified to calculate the displacement atom concentration and deposited energy density [5]. The SiC_f/SiC composite specimens were irradiated by a cyclic 14-MeV electron beam, the temperature was increased to the irradiation temperature 800°C by 14-MeV electron beam heating with the temperature increase rate of about 750°C/min and maintained for several minutes, then shut down. Many cycle irradiations on the specimen induce thermal fatigue and irradiation to simulate the cycle operation of fusion reaction. The experimental results show that:

1. Densification occurs with irradiation and the density of irradiated specimens approaching 2.800 g/cm^3.
2. The morphology of specimen surface was altered by irradiation. The morphology change for specimens is relative to irradiation temperature, the higher the irradiation temperature, the more change in the fiber morphology.
3. The resistivity change of 1D SiC_f/SiC composite is sensitive to the irradiation temperature; if the irradiation temperature is higher than 700°C, the resistivity change is not significant.
4. Irradiation on SiC_f/SiC composite induces the thermal diffusivity decrease.

The decrement of thermal diffusivity is not only sensitive to irradiation temperature, but also sensitive to the duration time of cycling operation. The interface damage between fiber and matrix occurs under the cyclic irradiation with short duration time. The irradiated specimens exposed by the laser beam simulate the thermal shock effects [16].The more serious the interface damage is, the more easily the specimen will melt. The region of matrix is easier to be melted than the fiber, which is shown in Fig. 2(a) and (b).

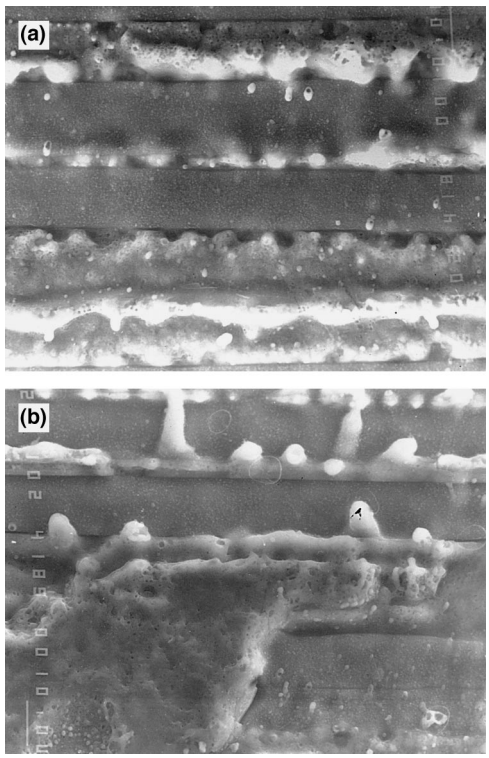

Fig. 2. The fiber and matrix in the melting region of SiC_f/SiC irradiated by the laser beam (magnification 1000×) (a) injection energy 10.18 MJ/M^2; (b) injection energy 17.18 MJ/M^2.

4. Tritium technology

The laboratory of tritium technology was established in CIAE to study the radiation performance of Al-Li alloy and $LiAlO_2$ and the coatings of preventing tritium permeation. A series of coating was carried out, such as TiC and TiN + TiC coated on the 316L SS by the PVD method and chemically heat treated to form the CH_4 barrier, $Al_2O_3$and SiC coating on 316L SS by magnetic control sputtering method and Al_2O_3 film coating on 305 aluminum alloy. The results indicate that the tritium permeability through the performed film coated on the surface of 305 aluminum alloy and the films of TiC and TiN + TiC coated on the surface of 316L SS, as well as Al_2O_3 and SiC coating on 316L SS, is 5–6 orders of

magnitude less than that of base materials. The TiC and TiN + TiC composite coating materials, after chemical heat treatment, are irradiated by 1 and 28 keV H^+ ions. After 1 keV H^+ ions beam irradiation to the fluence 3.1×10^{18} H^+/cm^2, the tritium permeability through TiC or TiN + TiC does not change. The tritium barrier is destroyed slightly and the tritium permeability through TiC or TiN + TiC increases by a factor of 3 with 28 keV H^+ ions beam irradiation, but it is still 4–6 orders of magnitude lower than that of the bulk. The tritium permeability through 316L SS with natural Al_2O_3 film increases by a factor of 247 after 1 keV H^+ ions beam irradiation to the fluence 2.8×10^{18} H^+/cm^2 [7–9].

5. Radiation effects on HTCS superconductor

The YBCO and Bi-system superconductor were irradiated by 20 and 35 MeV protons and the attached gamma rays at 70 and 30 K, the zero-resistance temperature T_{co} and critical current of specimens were measured in situ. T_{co} was increased with the fluence within the range (2.21×10^{13}–3.54×10^{14} p/cm^2). The increment of T_{co} was about 6–10 K and critical current was also enhanced [9,10]. The increment of T_{co} decay with the time after irradiation even if at low temperature, and one week later T_{co} becomes lower than the unirradiated value. An irradiation target chamber at low temperature associated with the HI-13 tandem accelerator was established and a special experiment was designed to discriminate the radiation effects on HTSC by γ ray and protons irradiation [12]. The fluorescent target on specimen 1 was irradiated by 20 MeV to produce γ ray. The fluorescent target was thick and the protons could not penetrate into specimen 1. The other three specimens were mounted on the other three faces of tetrahedron cool base. The T_{co} of specimens and the intensity of γ ray were measured respectively as time went on. The results are shown in Table 2. The increment of T_{co} is about 7 K at 1 h after irradiation; at this moment the intensity of γ ray is high. The T_{co} decreases gradually with the γ decay to reach the unirradiated value at 3 h after irradiation, at this moment the intensity of γ ray is 1/3 of that of 1 h after irradiation. Two months later, T_{co} decreases to the value about 3–5 K lower than that before irradiation.

There are two irradiation effects (ionization and displacement effects) on specimen by the proton and γ-ray irradiation. The excitation and ionization effect of proton and γ-ray irradiation produce many excited electrons and holes and high energy phonons in superconductor. These electrons and holes interact with phonons to form new superconductive carriers. The energy gap $\Delta(0)$ of new carrier pairs is higher than normal carrier pairs. The T_{co} of superconductor depends on the energy gap, which is $2\Delta(0) = 3.53\ K_B T_c$. If $\Delta(0)$ is larger than that of normal one, the T_{co} will be increased. This effect is instantaneous. The higher the γ ray intensity is, the more the density of abnormal superconductive pairs is, the more remarkable the change in T_{co}. From the experiment results, there is a saturated value of T_{co}. As γ ray intensity is increased over a certain level, T_{co} does not further increase. The displacement effects of proton and γ ray will produce defects in the superconductor and degrade the structure of the specimen to induce the T_{co} decrease. This effect is cumulative and depends on the γ rays' energy and fluences. At two months after irradiation, the ionization effects of γ ray is very weak and the T_{co} depends on the γ ray's fluences.

6. Theory and modeling of radiation damage processes

Nuclear reactions produced by D-T fusion neutrons will produce energetic atomic displacement cascades, helium and hydrogen gas and other transmutation impurity atoms: these will interact with the initial microstructure, modify it and thereby modify the bulk properties. We develop a physical model to take into account these factors and predict the microstructural evolution under irradiation. The main points of this physical model are the following:

(1) Inasmuch as part of interstitials are far apart from cascade by collision chains [13], cascade regions are the depleted zones (DPZ) and an interstitial-rich zone exists some distance from the primary event site. These regions are immersed in a host matrix which has an average vacancy, interstitial, transmutational helium concentration and transmutational impurity concentration.

(2) The helium atoms that are able to stabilize these depleted zones and vacancy clusters [14] evolve into bubble nuclei. The basic bubble nuclei are taken herein

Table 2
The change of T_{co} with time (h) after irradiating fluorescent target with 20 MeV protons

Specimen	T_{co} (K)			
	Before irradiation	1 h after irradiation	2 h after irradiation	3.5 h after irradiation
#1	107	112	110	107
#2	103	108	107	104
#3	106	112	110	108
#4	108	113	111	109

to be composed of two helium atoms plus a vacancy cluster. The bubble nucleation consists of four parts: first, the cascade regions have an associated helium to stabilize DPZ and another helium atom diffuses to this region to form two helium and several vacancies; second, a helium atom diffuses to a vacancy cluster and stabilizes it as a subnucleus and another helium atom diffuses into a subnucleus to form a nucleus; third, helium–helium interactions form bubble nuclei by homogeneous nucleation and fourth, the transmutational recoil helium atom remains in the cascade region it produced to form a subnucleus, and another helium atom diffuses into this region to form a nucleus.

(3) Two helium atoms combine with a vacancy cluster as a bubble nucleus, and the process of vacancy and helium migration into these nuclei are all named bubble growth processes. The bubble growth process satisfies a Langevin equation [15].

(4) The bubbles represent accumulated excess vacancies; the excess interstitial might be condensed interstitial clusters or loops. The interaction of impurities with interstitial leads to trapped interstitials. An assumption is made that three interstitials combining with an impurity atom form a stable interstitial cluster nucleus, and the process of interstitial migration into these nuclei is named an interstitial cluster (or loop) growth process. The interstitial cluster growth process also satisfies a Langevin equation and can be considered as a Markov process [15].

(5) The two processes, that of bubble evolution and of interstitial cluster evolution, are linked by vacancy, interstitial and helium concentration in the irradiated crystal. The vacancies, interstitials, helium and impurity concentration in the matrix govern the nucleation and growth processes; inversely, the interstitial, vacancy and helium concentration are calculated iteratively from a microstructural morphology which consists of bubble nuclei, bubbles, interstitial clusters (or dislocation loops) and a dislocation network at an irradiation time t [15].

According to this physical model a set of bubble and interstitial cluster evolution equations are established by the nonequilibrium statistical method. These equations describe the microstructural evolution, by which the computer program has been established. This computer program not only predicts the PIREX-I experimental results, but also reveals the whole evolution process, as well as the fluctuation coefficient and its behavior [15]. The calculated results, including bubble size distribution, interstitial cluster size distribution, helium concentration in matrix, bubbles and interstitial cluster nucleation rate, bubbles and interstitial cluster growth rate and evolution process, are all reasonable. The interstitial cluster distribution is shown in Fig. 3. Most of the interstitial clusters are less than 1 nm for PIREX-I experiments in aluminum, and their number is three orders of magnitude higher than the number of bubbles.

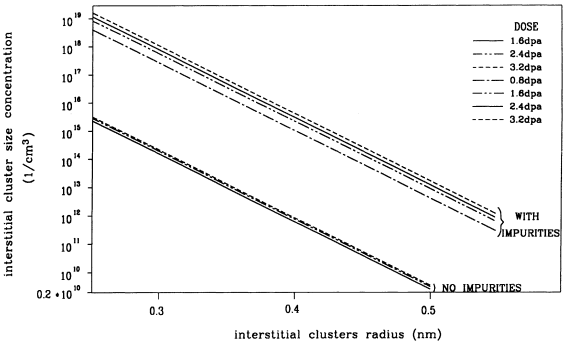

Fig. 3. Interstitial cluster concentration distribution (0.1 N_{Mg} and no impurities) for the aluminum specimen #102 irradiated by 600 MeV proton beam at 450 K. The 0.1 N_{Mg} is an effective impurity production rate.

This means that the interstitial clusters seem to be the hardening agent in irradiated aluminum. The impurities, Mg, and the fluctuation coefficient D_I play an important role for the interstitial cluster's evolution. If there is no impurities source, the number of interstitial clusters is four orders of magnitude less than that with impurities source [15].

7. Summary

CIAE emphasizes the study of radiation effects on the fusion materials, such as 316L SS, 316Ti SS, Cu-Al25 alloy, $LiAlO_2$, coatings of preventing tritium permeation, SiC_f/SiC composite and HTSC superconductors. In structural materials we emphasize the synergistic action of high-energy cascades, helium and hydrogen and modeling works.

References

[1] X. Zhao, Y. Chen et al., Chinese J. Nucl. Sci. Eng. 14 (1994) 58.
[2] J. Yu, Y. Chen et al., J. Nucl. Mater. 191–194 (1992) 728.
[3] J. Yu, Y. Chen et al., J. Nucl. Mater. 191–194 (1992) 818; Chinese J. Nucl. Sci. Eng. 14 (1994) 128.
[4] J. Yu, J. Chen et al., J. Nucl. Mater. 251 (1997) 150.
[5] J. Yu, J. Chen et al., J. Nucl. Mater. 233–237 (1996) 771.
[6] J. Li, H. Xu et al., Microstructural evolution in Cu-Al25 alloy under 300 keV Cu^+ ion irradiation, presented at 8th Int. Conf. on Fusion Reactor Materials (ICFRM-8), Sendai, Oct. 1997.
[7] C. Shan, J. Hao et al., Investigation of materials for preventing tritium permeation and resisting plasma irradiation, Proceeding of SJSMAES'95(59), 29 October–3 November 1995, Chendu, China.
[8] C. Shan, A. Wu et al., J. Nucl. Mater. 191–194 (1992) 221.
[9] J. Hao, C. Shan et al., Behavior of diffusion and permeation of tritium through 316L stainless steel coated with

Al_2O_3, Proceeding of SJSMAES'95(63), 29 October–3 November 1995, Chendu, China.
[10] J. Yu, Y. Wang et al., Chinese Phys. Lett. 12 (1990) 564.
[11] J. Yu, Z. Gao et al., Chinese Phys. Lett. 7 (1991) 368.
[12] X. Zhao, J. Yu et al., Chinese J. Nucl. Sci. Eng. 17 (1997) 227.
[13] J. Yu, Cascades and vacancy concentration induced by atomic collision in solid, Proc. of the 3rd China-Japan Metal Physics and Physical Metallurgy Symposium, 22–25 September 1988, p. 136.
[14] J. Yu, W.V. Green, M. Victoria, J. Nucl. Mater. 155–157 (1988) 1093.
[15] J. Yu, W.F. Sommer, J.N. Bradbury, J. Nucl. Mater. 141–143 (1986) 658; J. Yu, W.F. Sommer, J.N. Bradbury, ASTM STP 955 (1987) 393; J. Yu, W.F. Sommer et al., J. Nucl. Mater. 227 (1996) 266.
[16] J. Yu, W. Zhang et al., Thermal shock on the irradiated SiCf/SiC composite, Proceeding of IEA International Workshop on SiC/SiC Ceramic Composites for Fusion Structural Application, 28–29 October, 1996, Ispra, Italy.